

Numerical and Experimental Investigation of the Influence of Backpressure on a Confined Impinging Jet for Small Nozzle-to-plate Spacing

K. Zhu^{1†}, R. Shen¹, T. Sun¹, G. Cheng² and J. Ding³

¹ School of Mechanical Engineering and Rail Transit, Changzhou University, Changzhou 213164, China

² Institute of Intelligent Flexible Mechatronics, Jiangsu University, Zhenjiang, 212013, China

³ School of Mechanical Engineering, Yangzhou University 225009, China

†Corresponding Author Email address: zkq@cczu.edu.cn

ABSTRACT

In order to further extend understanding of the heat transfer characteristics under an enclosed area, the influence of backpressure on a single impingement jet with small nozzle-to-plate spacing (H/D) is studied. Particle image velocimetry (PIV) technique and a commercial fluid dynamics solver (CFD) are respectively employed to investigate the fluid dynamics of the impinging jet, with a Reynolds number (Re) of 3462–6125, at a small nozzle-to-plate spacing (H/D) of 0.25–1.25. Experimental data are in well agreement with numerical simulation data. The findings indicate that the H/D ratio significantly influences the formation of backpressure in the flow field. The backpressure then influences the boundary layer velocity on the impingement surface, in turn affecting the impingement surface's heat transfer characteristics. In addition, a turning point in the horizontal velocity curve of $H/D = 0.4$ is found for an entire range of jet heights, which is independent of the Reynolds number (Re).

Article History

Received July 8, 2023

Revised October 11, 2023

Accepted October 15, 2023

Available online January 1, 2024

Keywords:

Backpressure

Small nozzle-to-plate distances

Impingement cooling

Flow characteristic

Heat transfer performance

1. INTRODUCTION

The demand for ultra-slim glass has been steadily rising due to the continuous miniaturization of products such as solar photovoltaic modules and liquid crystal displays. To strengthen ultra-thin glass for production purposes, it undergoes a rigorous toughening process. This involves heating the glass to its melting point and subsequently rapidly cooling it using a fluid jet. Jet-impingement is a highly effective method for cooling hot surfaces. In many fields, jet impingement is commonly utilized for effective heat transfer from heated target plates. Several scholars have examined different types of heat transfer (Hussain et al., 2020; Thani & Ismael., 2022; Ismael et al., 2023; Hassan & Ismael., 2023), including impingement jet heat transfer and porous mass impingement jet heat transfer.

Most studies concentrate on large nozzle-to-plate spacings (Geers et al., 2005; Kalifa et al., 2016; Terzis, 2016; He & Liu, 2018; Pachpute & Premachandran, 2018; Lyu et al., 2019; Chang & Shen, 2020; Nagesha et al., 2019; Pachpute & Premachandran, 2020). For example, Choo et al. (2016) investigated the correlation between stagnation pressure and the Nusselt number in submerged jet impingement with giant nozzle-to-plate spacings. The

findings show that the Nusselt number of the plate exhibits a significant dependency on the stagnation pressure. Chen et al. (2019) explored the heat transfer performance of large nozzle-to-plate spacings ($H/D = 3.0-5.0$) on the jet impingement configuration. They concluded that decreased coverage of the regions with high heat transfer led to a reduction in the heat transfer coefficient within the wall jet area. Yu et al. (2018) investigated the heat transfer through jet impingement and its correlation for both a single jet and arrays of jet holes at varying distances ($H/D = 1.74-27.5$) between the nozzle and the plate. The heat transfer performance at the stagnation point of a single jet hole was close to that of two aligned rows of jet holes used for aircraft anti-icing applications. Tang et al. (2021) numerically simulated the dynamics of flow and heat transfer associated with a liquid jet striking the cylindrical cavity of a localized thermal source when H/D was 2. The heat transfer capacity of the radiator was increased using a cylindrical cavity structure. An oblique jet produced horseshoe vortices at the edge of the cavity, improving the cavity's heat exchange performance.

However, to date, there has been little research on small nozzle-to-plate spacings, including numerical simulation and experiment. Only Yu et al. (2017) have studied the heat transfer performance when $H/D = 0.2-1.0$. They found that the quenching time rapidly decreased

Nomenclature

D	nozzle diameter	v	fluid velocity
H	nozzle to impingement plate distance	V_m	inlet velocity
p	static pressure	x	distance along impingement plate length
Re	Reynolds number	y	distance along impingement plate height
T	temperature		

with decreasing H/D , which played a key role in toughening the ultra-thin glass. Choo and Kim (2010) explored the heat transfer of jet impingement at short spacings. The conclusions showed the independence of the Nusselt number from H/D (0.125-1.0) at a constant pump output. Kuraan et al. (2017) examined the heat transfer performance and fluid dynamics of water jet impingement when $H/D = 0.08-1.0$. The hydrodynamic jump diameter, pressure, and normalized Nusselt number over the entire H/D region were divided into two regions.

There was a change in pressure when the spacing from a nozzle to the target plate was under 1 ($H/D < 1.0$). Hadipour and Zargarabadi (2018) investigated the behavior of flow within the fluid domain and heat transfer performance of the circular jet (Frossell et al., 2018) impingement on a curved surface under small nozzle-to-plate spacings. Experimental measurements and numerical simulations indicated a substantial increase in the Nu , both in the axial directions and circumferential, when the distance between the nozzle and plate decreased to $H/D < 1.0$. Sexton et al. (2018) experimentally investigated the effects of varying nozzle aspect ratios on the fluid dynamic and thermal behavior of slit jets. Eccentric peaks were observed for slit jets with aspect ratios exceeding 1, resulting in saddleback behavior, making the authors speculate that the peaks were generated by backpressure (Qiu et al., 2016, 2018) effects in the stagnation zone. Zhao et al. (2022) experimentally investigated the restart process due to supersonic inlet backpressure. During startup, arising from increasing backpressure in inlet, the backpressure gradually moved upstream, across the region of boundary layer separation, which, in turn, influenced the entire vibration insulator. The backpressure affected the separation region, separation point, and finally, the impact angle. Yeom et al. (2019) studied the influence of the distance between the jet orifice and a fin tip. Studies have shown that a synthetic jet (Zhang et al., 2018; Gil & Wilk, 2020) can cool the fin tips more effectively when the separation distance is small. The above studies show that backpressure influences jet heat transfer, especially at small spacings. Therefore, it is essential to study backpressure for small nozzle-to-plate distances in terms of heat transfer by jet impingement.

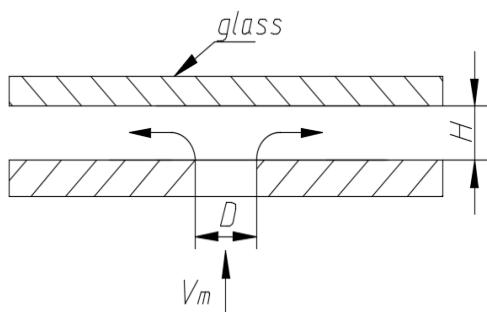


Fig. 1 Physical model of single jet impingement

We investigate the influence of backpressure on a single impinging jet for small nozzle-plate spacings. For different Reynolds numbers ($Re = 3462-6125$) and different nondimensional nozzle-to-plate distances ($H/D = 0.2-1.25$), the backpressure distribution and flow field structure are examined using PIV and numerical simulation to determine how backpressure affects heat transfer characteristics. An in-depth explanation of the experiment and simulation precedes the analysis of the results.

2. CFD AND EXPERIMENTAL METHODS

We examined the influence of backpressure on small nozzle-to-plate distances at room temperature via simulation and experiment. The commercially available fluid dynamics solver Fluent 15.0 was utilized to perform the numerical simulation of the matter, energy, turbulence, and flow equations. The pressure-velocity coupling was resolved utilizing a SIMPLEC algorithm. Discretization of velocity, pressure, and temperature was conducted using a second-order windward approach. The second-order upwind approach has second-order accuracy. Compared to the first-order upwind approach, the second-order upwind approach can provide higher numerical accuracy and better stability. It can effectively reduce the accumulation of numerical errors when dealing with flow problems with strong convection effects. An implementable SST $k-\omega$ turbulence model was incorporated into the simulation to better handle the flow calculation process in the near-wall region, and to obtain a more accurate description of the turbulence dynamics. The internal flow field of a small pitch jet was observed using the PIV technique. A Kingder dual-pulse laser ($2 \times 200 \text{ mJ} @ 532 \pm 1 \text{ nm}$) was used for illumination, and the optical thickness was 1 mm. An Imperx high-speed digital camera and a Nikon macro-lens with an imaging resolution of 2048×2048 were used for imaging. Tracer particles, possessing a diameter approximately around $10 \mu\text{m}$, were injected by a smoke generator at the fan inlet and mixed in a steady flow device for the experiments. We simulated the influence of backpressure on jet heat transfer at high temperatures.

2.1 Simulation Method

2.1.1 Geometry

The physical geometry was that of a confined impact jet, as can be seen in Fig. 1. The diameter of the circular jet, D , remains constant at 4 mm, and there is a range of 1 to 5 mm between the nozzle and the glass. V_m represents the inlet velocity of the jet nozzle, and the jet impact parameters are shown in Table 1.

Figure 2 illustrates the geometry of the computational model of single jet impingement, with the lower half being the fluid domain and the upper half being the solid domain, composed of glass. Air impinges vertically through a round tube on the glass plate having dimensions of 100mm,

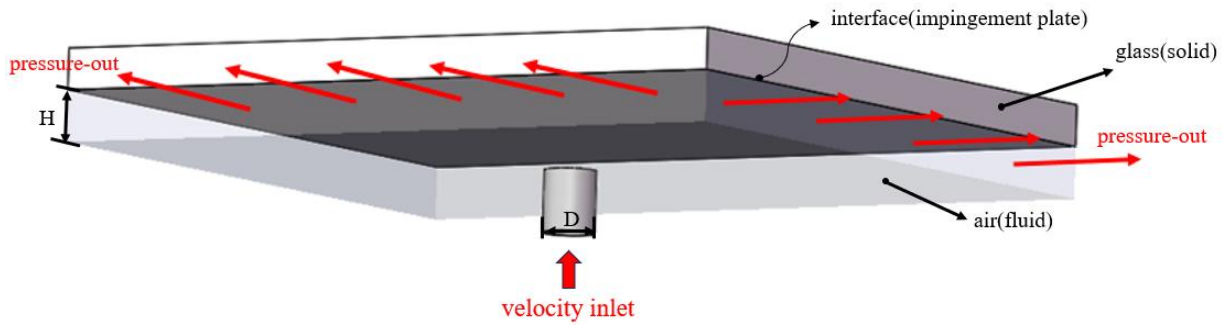


Fig. 2 Computational model of single jet impingement

Table 1 Parameters of numerical and experimental settings

Parameter	Setting
H/D	0.25, 0.5, 0.75, 1, 1.25
Re	3462, 5326, 6125
V_m (m/s)	13, 20, 23

100mm, and 2mm. The jet inlet is circular to maximize heat transfer efficiency. During glass tempering, not only does the surface temperature exhibit non-linear changes with respect to time, but there are also substantial changes in the material properties as the temperature increases. The glass density is set at 2500 kg/m³ and the glass plate is initially set at a temperature of 953K. In our research, we explore the transient heat transfer characteristics between a glass (solid) and air (fluid) domains using conjugate heat transfer.

2.1.2. Grid Independence Analysis

The whole structural mesh domain was formed utilizing the O-block functionality provided by the software package ANSYS ICEM CFD 15.0. To enhance the grid quality, mesh refinement was performed for the fluid domain and the glass plate region, as displayed in Fig. 3. To meet the requirements of the SST k- ω turbulence model, the y^+ value, representing the dimensionless wall distance at the first node, is less than 1, and the minimum size of the near-wall is 2.55e-06 m, which otherwise varies with the jet Reynolds number. In line with previous work (Yu et al., 2017), Fig. 4 illustrates the grid independence investigation, depicting the relationship between the glass surface temperature and the quenching time, at $Re = 30000$ and $H/D = 1$. We completed the grid independence check by considering different grid systems. Figure 4 shows that the grid range is between 285014 and 676704, and that the variance in glass surface temperature is below 1%. Therefore, we selected a grid number of 478940 to ensure fine-resolution grid independence results and heat transfer distribution results.

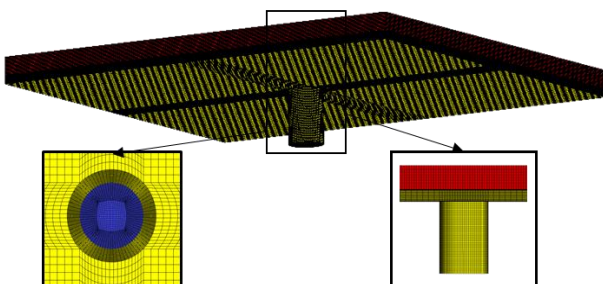


Fig. 3 Mesh of the computational domain for $Re = 6125, H/D = 0.25$

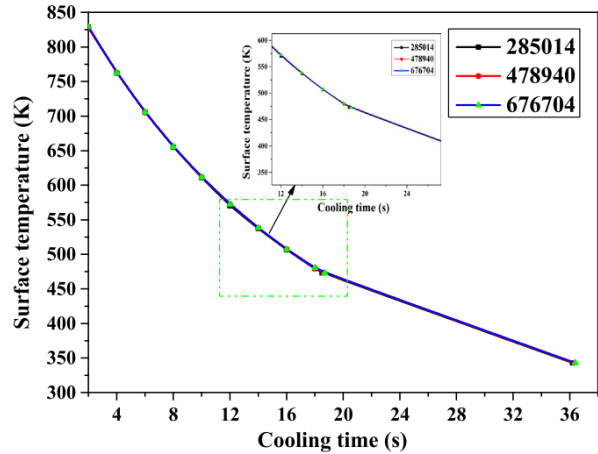


Fig. 4 Grid independence verification

2.1.3. Governing Equations

The equations governing the transient transport of mass, momentum, and energy are as follows:

$$\frac{\partial \rho}{\partial t} + \nabla \cdot (\rho u) = 0 \tag{1}$$

$$\frac{\partial}{\partial t} (\rho u) + \nabla \cdot (\rho u u) = \nabla (\bar{\tau}) - \nabla p \tag{2}$$

$$\frac{\partial}{\partial t} (\rho I_t) + \nabla \cdot (u(\rho I_t + p)) = \nabla \cdot (\lambda \nabla T + (\bar{\tau} \cdot U)) \tag{3}$$

In the given equations, u is the velocity, ρ is the density, P is the pressure, I_t is the total enthalpy, λ is the thermal conductivity, and $\bar{\tau}$ is the stress tensor.

2.1.4. Boundary Conditions

(1) Nozzle: It is designated as the inlet where the air is ejected at a uniform velocity and varying Reynolds number, with a turbulence intensity equal to 5% of the flow rate. The temperature at the jet inlet remains constant at 298 K.

In the majority of jet impact investigations, the impact Reynolds number is ascertained using the volumetric mean of the jet, which is defined as follows:

$$Re_j = \frac{u_j d_j}{\nu} = \frac{4 \dot{m}}{N \pi \mu d_j} \tag{4}$$

where \dot{m} is the total mass flow rate, N is the number of nozzles, d is the jet diameter, u_j is the inlet velocity, μ is the dynamic viscosity, and ν is the kinematic viscosity.

(2) Lower wall: The air fluid domain's wall has no slip and is adiabatic.

$$\text{At } Z = H, -\frac{L}{2} \leq X \leq \frac{L}{2} \text{ and } -\frac{W}{2} \leq Y \leq \frac{W}{2}$$

$$\frac{\partial T}{\partial z} = 0 \quad (5)$$

(3) Outlet boundary for flow rate: The flow outlet equates to the pressure outlet, where the pressure is recognized to be atmospheric pressure.

(4) Impingement plate: The lower section equates to the border of fluid-solid coupling. The rest of the plate forms the convective heat transfer coefficient boundary.

(5) Initial condition: When the initial cooling time t equals to 0, fluid enters through the nozzle, and the glass's surface temperature dropped. The solid domain (glass) begins with a temperature set at 953K.

2.1.5. Flow Solver

Common turbulence models of impinging jet heat transfer include the realizable SST $k-\omega$ model, V^2F model, $k-\epsilon$ model, and large eddy simulation model. The SST $k-\omega$ turbulence model can better handle the flow calculation process in the near-wall region and has wide applicability and high calculation accuracy. This model is also widely recognized as good for studying near-wall flow regions (Huang et al., 2019). In our previous research (Yu et al., 2017), the applicability of this model for an impingement jet flow field with small nozzle-to-plate spacings was verified. Therefore, this paper uses the SST $k-\omega$ turbulence model to study the impact of small-pitch jet heat transfer. In the SST $k-\omega$ model, the inlet temperature, outlet temperature, and fluid domain temperature are set to the ambient temperature. It is assumed that the fluid is three-dimensional, incompressible, and turbulent, with the wall designated as adiabatic and no-slip. The impacts of radiative heat transfer and buoyancy are neglected in the numerical simulation.

2.2 Experimental Method

2.2.1 Test Facility

The system designed according to the experimental schematic diagram is mainly composed of a centrifugal fan, a flow valve, a flow stabilization device, an air tank, an orifice plate, an electric control cabinet, a three-dimensional sliding table, and a PIV test system, as shown in Fig. 5. The airflow provided by the fan is controlled by the flow valve, and the flow stabilization device stabilizes the flow before it hits the glass plate after traveling vertically upward through the nozzle on the plate. The flow stabilization device comprises a honeycomb design to ensure that the error in the outflow speed for each nozzle hole is $\pm 2.5\%$. Single-hole orifice plate opens circular holes that have a diameter of 4 mm ($D = 4$ mm). The height, H , of the jet from the impinging plate to the orifice plate is fine-tuned by a three-dimensional slide lifting frame with an accuracy of 0.1 mm. The glass plate translation speed accuracy is 1 mm/s.

2.2.2 PIV Technique

During the filming process, Fig. 6 illustrates the schematic representation of image capture. The laser

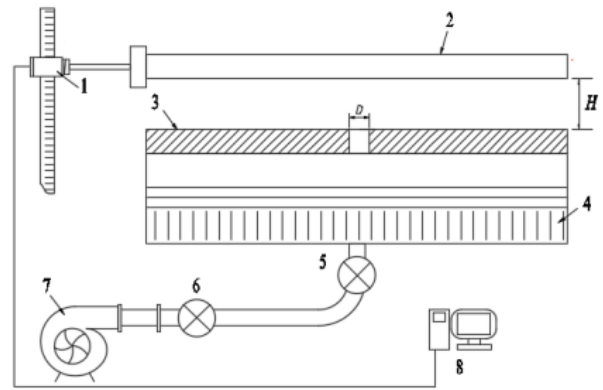


Fig. 5 Schematic diagram of the experimental device: 1. three-dimensional moving slide, 2. glass, 3. replaceable orifice plate, 4. stabilizing device, 5. flow meter, 6. ball valve, 7. fan, and 8. computer

strikes the perforated plate through the glass from directly above the glass that is to be measured. The sheet light coincides with the longitudinal symmetry plane of the perforated plate. A CCD camera is placed outside the device and captures the flow field in the cut plane perpendicular to the light plane. The shooting object is the flow field illuminated by the laser light in the gap between the orifice plate and the glass plate in Fig. 6. Taking the center of the orifice plate's surface as the origin, O , a rectangular coordinate system (as shown in Fig. 6) is established in the two-dimensional flow field region. The shooting flow interval is $-70 \text{ mm} \leq x \leq 70 \text{ mm}$, $0 \leq y \leq H$, where H is the small pitch height of the jet studied in this paper, whose range is $0.25 \leq H/D \leq 1.25$. Each group of experimental data consists of 100 frames of continuous instantaneous images. These digital images are processed using the commercial software DynamicStudio.2015a. The calculation parameters are selected according to the measured flow field area to obtain the velocity vector field (Table 2).

2.3 Verification

To validate the model's accuracy, the commercial software FLUENT was used to numerically simulate the flow field of a single jet impingement on the glass plate for $Re = 3462$, $H/D = 1$. In order to verify the numerical

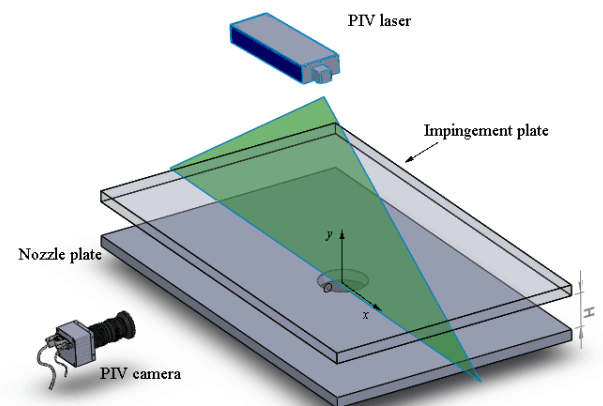


Fig. 6 Schematic diagram of the test section and PIV camera location

Table 2 PIV parameters

H/D	Parameter	Setting
0.25	Calculation area (mm ²)	70 × 0.8, 70 × 1
	Grid settings	Adaptive PIV 8 × 8 px ² ~16 × 16 px ² Step size 4 × 4 px ²
	Moving average validation	Averaging size 7 × 3 px ²
		Acceptance factor 0.1
		Iteration times 3
0.5,0.75	Calculation area (mm ²)	70 × 2, 70 × 3
	Grid settings	Adaptive PIV 16 × 16 px ² ~24 × 24 px ² Step size 8 × 4 px ²
	Moving average validation	Averaging size 5 × 3 px ²
		Acceptance factor 0.1
		Iteration times 3
1,1.25	Calculation area (mm ²)	70 × 4, 70 × 5
	Grid settings	Adaptive PIV 16 × 16 px ² ~24 × 24 px ² Step size 8 × 8 px ²
	Moving average validation	Averaging size 5 × 3 px ²
		Acceptance factor 0.1
		Iteration times 3

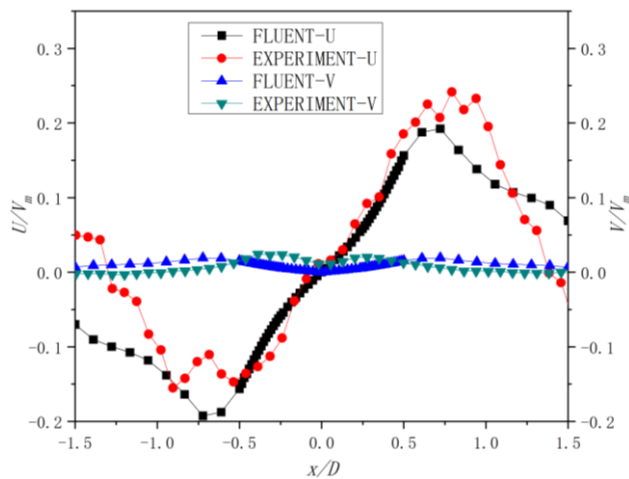


Fig. 7 Comparison between the simulation and experiment for $Re = 3462$, $H/D = 1$

simulations, a jet velocimetry test rig was constructed, as shown in Fig. 6. This consisted of a stand, a fan, a PIV system, and a glass plate to obtain the flow's velocity vector field. The vertical component V and horizontal component U of the calculated boundary layer velocity were compared with the experimental data from room temperature under this condition. Figure 7 indicates a substantial alignment between the outcomes of the simulation and the experimental results. Therefore, this model can accurately capture numerically the small-pitch jet flow field.

3. RESULTS AND DISCUSSION

3.1 Backpressure Distribution

Figures 8 and 9 show results for the backpressure distribution for different Re numbers at $H/D = 0.25$ and for different H/D values at $Re = 6125$, respectively. The flow fields all generate backpressure, independent of the value of Re . Figure 8 shows that, for $H/D = 0.25$, the backpressure increases with increasing Re , leading to an expansion of the core region. Figures 8(c) and 9 show that,

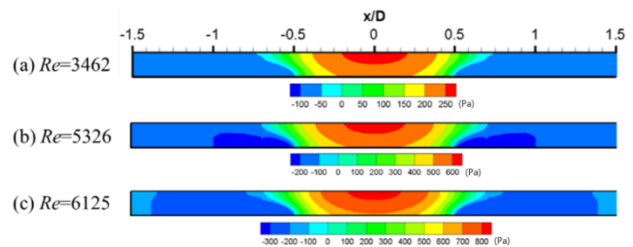


Fig. 8 Numerical plots of backpressure distribution (Pa) for different Re numbers at $H/D = 0.25$

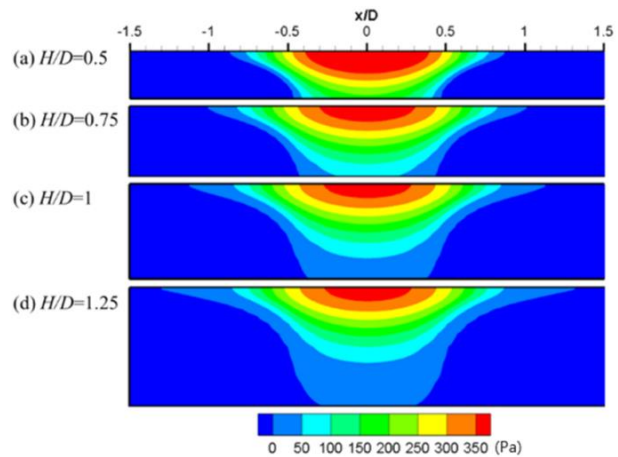


Fig. 9 Numerical plots of backpressure distribution (Pa) for different H/D values at $Re = 6125$

for $Re = 6125$, the peak backpressure developed in the nozzle axis decreases rapidly with increasing H/D , resulting in a reduction in the high-pressure area covered.

3.2 Outlet Velocity

To investigate the effect of H/D on the flow field, a comparison was made between the simulation and experimental results. The outlet velocity, V_e , normalized by the inlet velocity, V_m , for different H/D values and $Re = 6125$, is plotted in Fig. 10. Both sets of results are symmetrical around the central axis of the jet. The left half

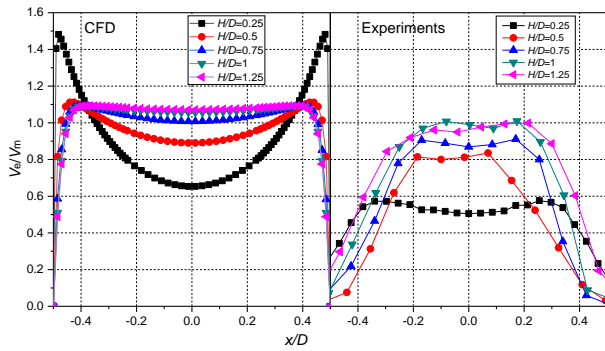


Fig. 10 Numerical and experimental curves of normalized outlet velocity for different H/D values at $Re = 6125$

of Fig. 10 shows the outlet velocity amplitude plotted for numerical simulations of turbulent impinging jets under different confined heights ($H/D = 0.25-1.25$) for $Re = 6125$. The right half of Fig. 10 depicts a plot of the magnitude of the outlet velocity measured by PIV for the same operating conditions. Both results indicate that the decrease in velocity at the stationary point affects the distribution of the outlet velocity near the nozzle axis. This is caused by the backpressure, which is mainly influenced by H/D .

We now examine in detail the outflow velocity near the nozzle ($|x/D| \leq 0.5$) for different restriction heights ($0.25 \leq H/D \leq 1.25$). The numerical simulation results and experimental results in Fig. 10 show that, as the normalized spacing H/D decreases, the value of the outlet has a depression at the stationary point ($x/D = 0$) and a maximum near the nozzle boundary. According to the results shown in the left panel of Fig. 10 (CFD plot), the velocity distribution for the normalized spacing $H/D = 0.25$ is significantly different from that of the other confined heights, with the velocity at its stationary point decaying to a trough at the jet centerline ($0.65 V_m$), while the peak velocity at the nozzle boundary ($|x/D| = 0.5$) ($1.4 V_m$) far exceeds the maximum value ($1.1 V_m$) at the other

confined heights. Comparing the right panel of Fig. 10 (experimental plot) displays that the results for the outlet velocity near the nozzle axis align well with the simulation results, and follow the same laws as those obtained from the simulation. However, the experimental results for the nozzle boundary are different from the simulation results. This is due to limitations in the measurement technology. H/D is too small in the experiments for the oil droplets to be used as tracer particles because of its effect of gravity, affecting the measurement results. Therefore, the horizontal velocity, U , in the near-wall area is used to further prove the objectivity of the law in subsection 3.4.

The phenomenon is due to the glass plate creating considerable backpressure within the flow field. Figures 8–10 show that the pressure is high near both the nozzle axis and the glass surface compared with the surrounding environment. Therefore, the fluid at the center of the nozzle has the smallest outlet velocity under the growing influence of backpressure. In the radial direction, the deceleration effect on the fluid gradually weakens as the backpressure decreases. When H/D is large, the backpressure at the nozzle axis is small, and the deceleration effect on the fluid is limited. However, for $H/D = 0.25$, the backpressure is much higher than that of the other small spacings ($H/D = 0.5-1.25$). At the same time, due to mass conservation, the outflow rate near the nozzle boundary increases sharply. Notably, this is why the outlet velocity is much larger than the inflow velocity when $H/D = 0.25$.

3.3 Flow Characteristics

To study the influence of backpressure on flow characteristics, the field of the flow for different H/D values at $Re = 3462$ and for different Re numbers at $H/D = 0.25$ was studied. The results are shown in Figs. 11 and 12, respectively. The left side of the diagram informs the velocity magnitude contours and streamlines obtained using the CFD results, while the right side of the diagram informs the velocity vectors obtained using the PIV results. The simulation and experimental results agree well.

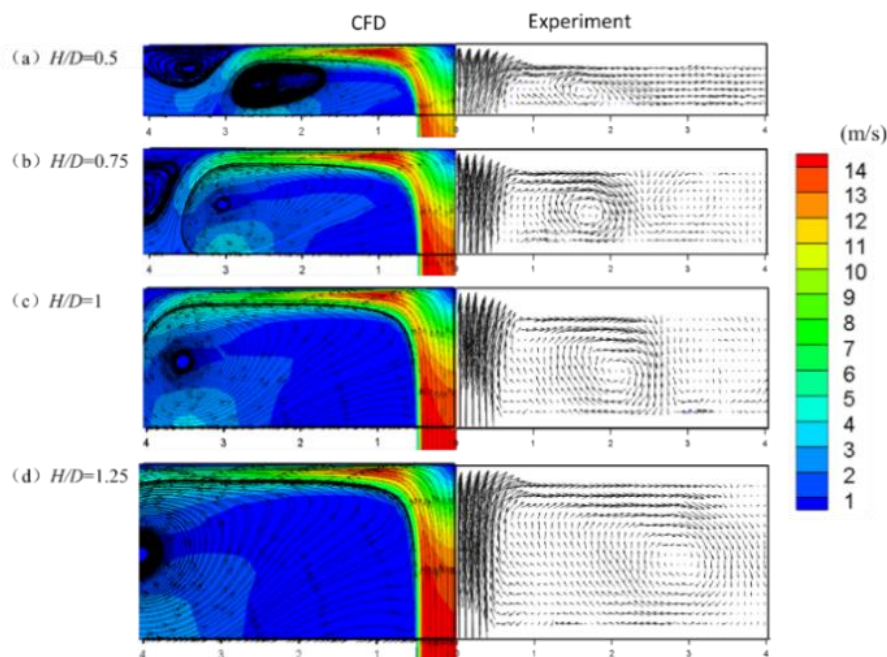


Fig. 11 Velocity magnitude plots of the flow for different H/D values at $Re = 3462$

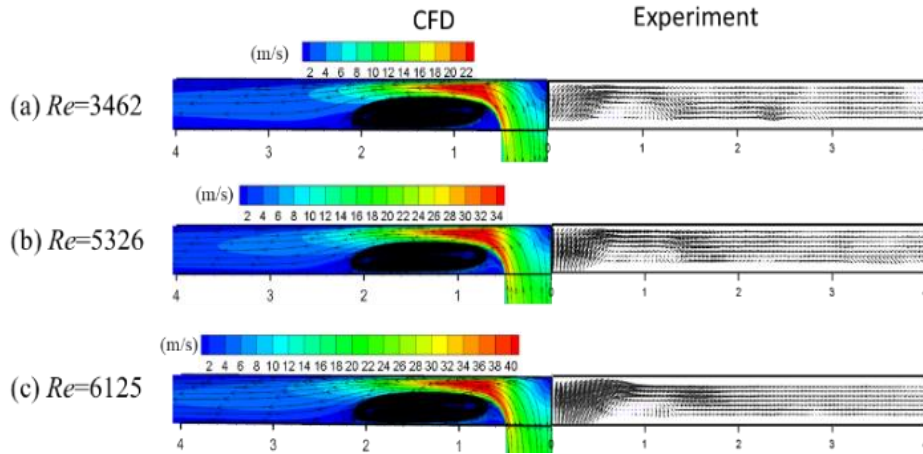


Fig. 12 Velocity magnitude plots of the flow for different Re numbers at $H/D = 0.25$

Figure 11 shows that, as the jet impinges on the glass plate, the axial velocity component decelerates, causing the jet to radially spread outward. This leads to the development of a wall jet adjacent to the impinging surface. When in the stagnation zone there is no positive pressure gradient, a hydrodynamic and thermal boundary layer develops between the impinging surface and the wall jet and begins to develop and thicken. As the jet expands radially outward, a reverse pressure gradient is formed, causing the wall jet to reach a critical point where its momentum fails to override the effect of gravity and the reverse friction from the impingement surface. This results in the wall jet to separate from the target surface and descend downward, and, because of the nozzle's coiled suction effect, a circular vortex is formed. As H/D increases, the pressure of the outlet decreases rapidly, which increases the pressure differential between the stagnation point and the outlet. Now, the vortices begin to appear in pairs.

When $H/D = 0.25$ (Fig. 12(a)) the outlet flow line aligns parallel to the impact plate, allowing it to be treated as a pipe flow. The vortex is only present near the nozzle and does not extend throughout the entire fluid domain (Fig. 11). Also, the maximum fluid velocity is observed in the range $0.75 < x/D < 1.5$ for $H/D = 0.25$. With the Re grows, the maximum velocity increases, and at a Reynolds number of 6125, the wall flow lines are perfectly parallel to the impact plate (experimental diagram in Fig. 12(c)). The turbulent energy of the jet is enhanced, resulting in a higher convective heat transfer capacity, which leads to a lower surface temperature and shorter quenching time.

3.4 U -velocity of the Boundary Layer of Impinging Surface

To better grasp the influence of H/D on the flow field, we used the simulation and experimental data to obtain the tangential component of the boundary layer velocity, U , normalized by the inlet velocity V_m . with different H/D at $Re = 3462, 5326,$ and 6125 is plotted in Fig. 13. The simulation and experimental results agree well.

When fluid is ejected from the nozzle, the centerline of the jet maintains the velocity and direction of the outlet, and the jet approaches the impact plate. The tangential velocity, U , is always 0 at the stationary point and increases along the radial direction before reaching a

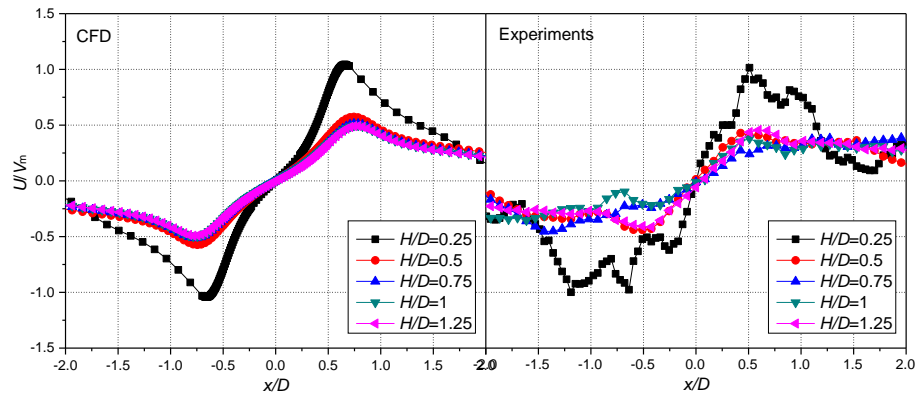
maximum near the nozzle boundary ($|x/D| = 0.5$). For $H/D = 0.25$, the maximum value of U can reach, or even exceed, the inlet velocity and far exceeds the maximum value of other H/D under the same Re (not exceeding $0.5 V_m$).

Figure 14 shows sorted and fitted horizontal component peak data for different H/D values. H/D considerably influences the extreme value, U_{max} , of the boundary layer flow velocity on the glass surface, which is independent of Re . In the entire jet height range, there is a turning point, $H/D = 0.4$, which is reported elsewhere (Kurraan et al., 2017). When $H/D \geq 0.4$, U_{max} is less affected by the backpressure, and its value does not exceed $0.5V_m$. When $H/D < 0.4$, the greater the effect of backpressure is as H/D decreases, the U_{max} increases sharply, where its value can reach several times of the incident flow velocity.

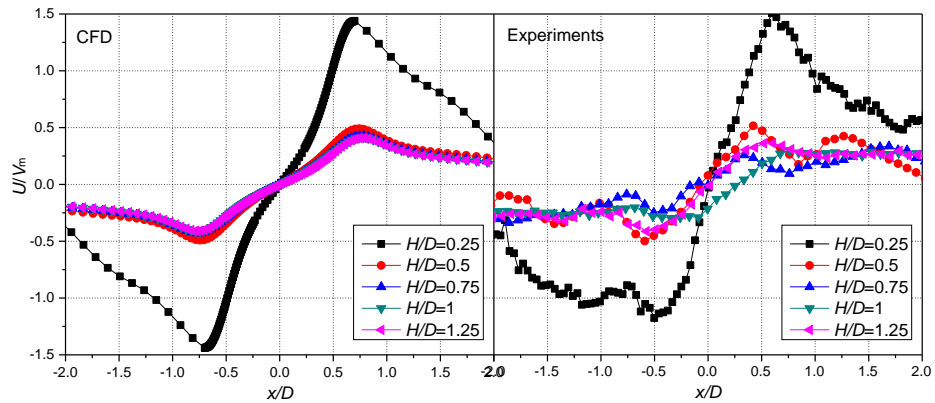
3.5 Effect of Backpressure on Heat Transfer

To further investigate the effect of backpressure on heat transfer, the instantaneous surface temperature at different H/D values and at $t = 6$ s and $Re = 6125$ was investigated (Fig. 15). The backpressure affects the fluid structure of jet impingement in a confined space, which promotes heat transfer on the glass surface. A low-temperature region always appears at the stationary point, especially, when $H/D = 0.25$ (Fig. 15(a)), the temperature at the region of the stationary point is the lowest, and there is no high-temperature region on the glass surface, and the temperature exhibits a uniform distribution, so the cooling effect is better. This is because the backpressure is much higher for $H/D = 0.25$ than for the other small spaces ($H/D = 0.5-1.25$). The increase in backpressure results in a substantial surge in the U -velocity of the boundary layer on the impinging surface and a faster temperature drop on the impinging surface, enhancing the heat transfer capability.

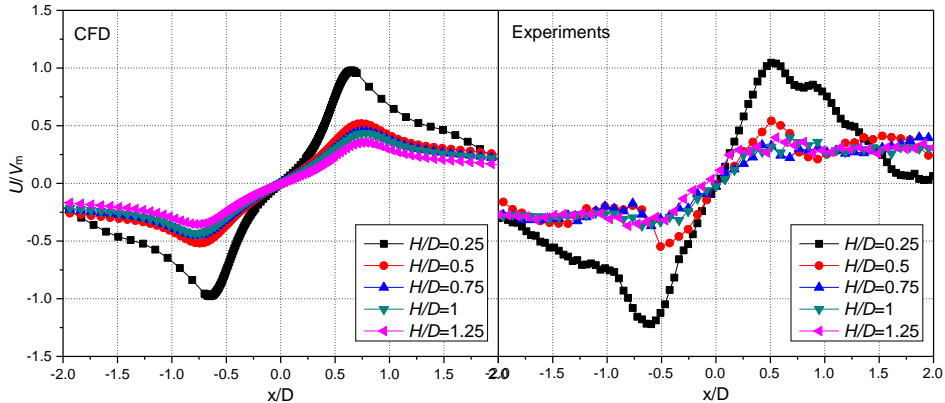
In addition, over the entire range of confined heights ($0.25 \leq H/D \leq 1.25$), on the glass surface, the regions of highest temperature occur for $H/D = 0.5$ (Fig. 15(b)). Figure 16 shows that the average temperature of the glass surface at $H/D = 0.5$ is consistently high as Re increases. Combining Figs. 15(b) and 16 shows that the glass surface at $H/D = 0.5$ has the worst heat transfer effect. This confirms that $H/D = 0.4$ is a turning point in terms of heat



(a) $Re = 3462$



(b) $Re = 5326$



(c) $Re = 6125$

Fig. 13 Normalized U -velocity profiles for different Re numbers and H/D values

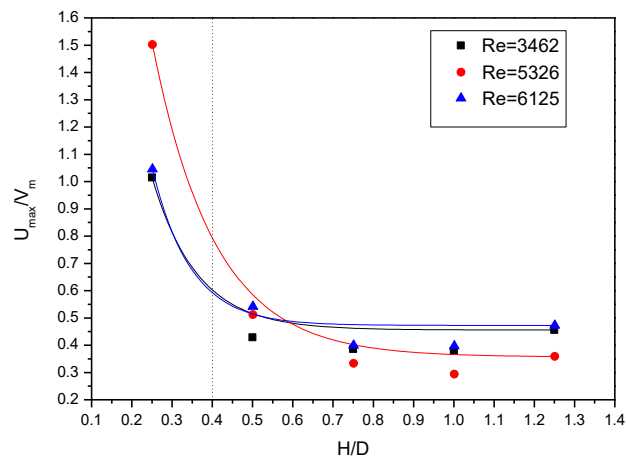


Fig. 14 Normalized maximum U -velocity of the boundary layer on the impinging surface obtained using PIV results on H/D

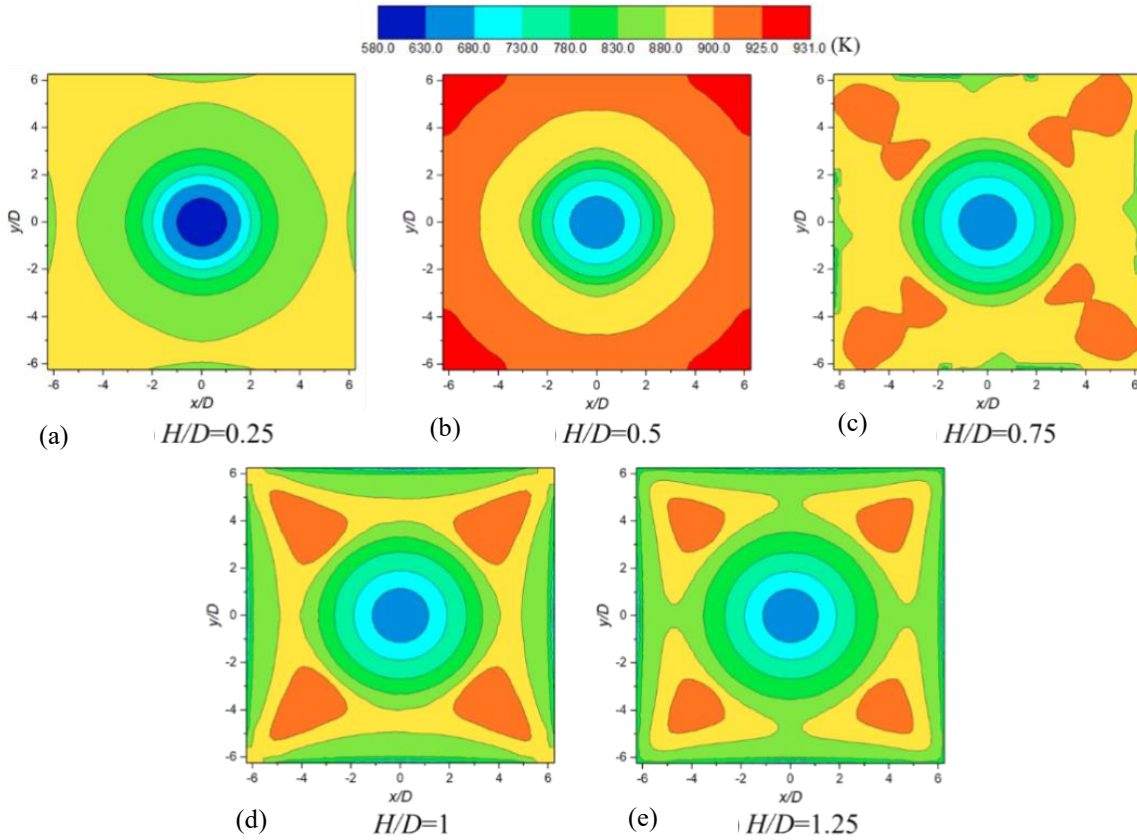


Fig. 15 Contours of transient impinging surface temperature for different H/D values when $Re = 6125$ and $t = 6$ s

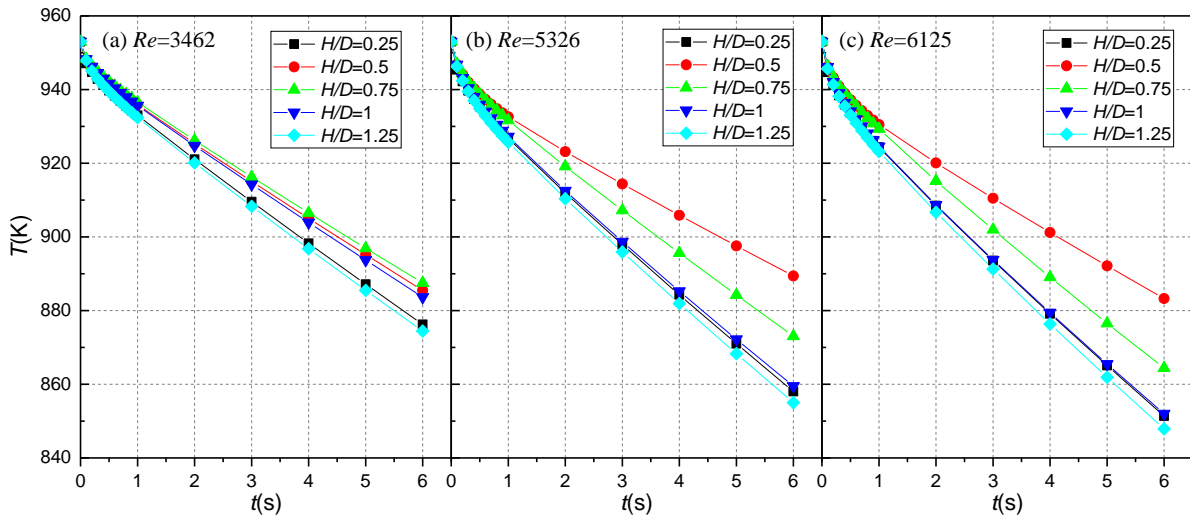


Fig. 16 Average impinging surface temperature with cooling time

transfer efficiency. Figure 14 shows that, when H/D decreases from 0.4 to 0.25, the greater the influence of backpressure, the greater the value of U_{max} , which significantly enhances the convective heat transfer capacity. When $H/D > 0.4$, U_{max} is less influenced by backpressure and decreases significantly, resulting in a decrease in the convective heat transfer capacity. However, although U_{max} remains almost constant when H/D increases from 0.75 to 1.25 (Fig. 14), the high-temperature region on the glass surface decreases in size substantially (Figs. 15(c)–15(e)). This means that the heat transfer effect is improved considerably by increased nozzle-to-plate spacing. Figure 16(c) shows that the cooling rate for

$H/D = 1$ is almost the same as that for $H/D = 0.25$. The increased gap between the plate and the nozzle leads to greater heat dissipation space, thereby improving the heat transfer capability of the jet impingement.

Figure 16 depicts the average impact surface temperature as a function of quenching time under different H/D values and $Re = 3462$, 5326, and 6125. H/D plays a substantial role in the heat transfer performance of the glass surface, which is independent of Re . In addition, the needed Re drops sharply for small H/D values at a given rate of cooling. For example, the average temperature on the surface of the glass plate decreases to approximately 900 K in under 4 s for $Re = 3462$ and H/D

= 0.25 instead of $Re = 6125$, $H/D = 0.5$. This means that the fluid mass decreases by 43.5% to achieve the same cooling effect simply by reducing H/D under the same working conditions and equipment conditions. From an environmental point of view, backpressure saves physical space in the cooling process, considerably reducing energy costs, such as electricity costs and exhaust gas emission costs, while achieving significant heat transfer efficiency. The proper utilization of backpressure has a noticeable influence on the transition of flow regime, such as the conversion from turbulent to laminar flow. It can not only reduce production costs, but also improve productivity to achieve the effect of energy saving and emission reduction. This addresses the issue of low heat transfer efficiency and suboptimal energy utilization in the existing cooling process. It lays a conceptual foundation for future structural designs of the cooling process by allowing adjustment of either the distance between the nozzle and the target plate or the nozzle diameter.

4. CONCLUSION

The present research delves into a comprehensive exploration of the impact of backpressure on a confined impinging jet characterized by a small nozzle-to-plate spacing. The research contributes valuable insights into the intricate realm of heat transfer dynamics within enclosed areas. A harmonious convergence between the numerical simulation data and the empirical evidence bolsters the reliability and robustness of the outcomes. Central to the investigation, meticulously account for critical variables, notably the H/D ratio and Reynolds number, thereby enhancing the depth and precision of the analysis. Notably, an inflection point in the horizontal velocity curve is discerned, exhibiting a remarkable independence from the Reynolds number, thereby elucidating a novel aspect of the impinging jet's behavior. In totality, this study augments the theoretical framework underpinning jet impingement applications, thereby enriching the comprehension of heat transfer phenomena in confined spaces. Based on the above results, the conclusions are as follows:

(1) For small spacings ($H/D = 0.25-1.25$), the backpressure produced a substantial increase in the velocity of the impact surface boundary layer, which exceeded the inlet velocity by a large margin. When H/D decreased to 0.25, the peak velocity at the nozzle boundary ($|x/D| = 0.5$) reached $1.4 V_m$, far exceeding the maximum value at the other constrained heights.

(2) The particular phenomenon of the distribution of both jet velocity and the horizontal velocity U in the near-wall area was related to the backpressure only, and not Re .

(3) Within the entire nozzle-to-plate spacings range ($H/D = 0.25-1.25$), there exists a turning point in quenching time at $H/D=0.4$, which was independent of Re . The U -velocity at the boundary layer of the impact surface increases by more than a factor of 1.5 when H/D decreased from 0.4 to 0.25; however, the U -velocity at the boundary layer of the impact surface nearly remains constant when H/D decreased from 0.4 to 1.25.

This research was conducted under high flow rate and confined space conditions, and the results have evident applicability in certain industrial fields such as ultrathin

tempered glass production. However, with the development of modern technology, research environment in other relevant fields is becoming increasingly demanding, approaching high flow rate and confined space conditions. The conclusions of this research provide theoretical basis and predictions for related industries and technologies. In subsequent studies, we will explore in depth the potential value of jet impingement technology in wider application scenarios, such as the application prospects of vane-shaped vortex generators in aerospace engineering.

ACKNOWLEDGEMENTS

This study was supported by the National Natural Science Foundation of China (Grant No. 51905049).

CONFLICT OF INTEREST

The authors declare that there is no conflict of interest.

AUTHORS CONTRIBUTION

Keqian Zhu: played a significant role in formulating the research idea; **Ruyi Shen:** conducted the experiment; **Tao Sun:** made substantial contributions to the analysis and preparation of the manuscript; **GuangGui Cheng:** carried out the data analysis and authored the manuscript; **Jianning Ding:** assisted in conducting the analysis through valuable discussions.

REFERENCES

- Chang, S. W., & Shen H. D. (2020). Heat transfer characteristics of swirling impinging jet-arrays issued from nozzle plates with and without webbed grooves. *International Journal of Thermal Sciences*, *148*, 106155. <https://doi.org/10.1016/j.ijthermalsci.2019.106155>
- Chen, L. L., Brakmann, R. G. A., Weigand, B., Crawford, M., & Poser, R. (2019). Detailed heat transfer investigation of an impingement jet array with large jet-to-jet distance. *International Journal of Thermal Sciences*, *146*, 106058. <https://doi.org/10.1016/j.ijthermalsci.2019.106058>
- Choo, K. S., & Kim, S. J. (2010). Heat transfer characteristics of impinging air jets under a fixed pumping power condition. *International Journal of Heat and Mass Transfer*, *53*, 320–326. <https://doi.org/10.1016/j.ijheatmasstransfer.2009.09.027>
- Choo, K., Friedrich, B. K., Glaspell, A. W., & Schilling, K. A. (2016). The influence of nozzle-to-plate spacing on heat transfer and fluid flow of submerged jet impingement. *International Journal of Heat and Mass Transfer*, *97*, 66–69. <https://doi.org/10.1016/j.ijheatmasstransfer.2016.01.060>
- Frosell, T., Fripp, M., & Gutmark, E. (2018). Dynamics of the impingement region of a circular turbulent jet. *Experimental Thermal and Fluid Science*, *91*, 399–409. <https://doi.org/10.1016/j.expthermflusci.2017.10.02>

7

- Geers, L. F. G., Hanjalic, K., & Tummers, M. J. (2005). Wall imprint of turbulent structures and heat transfer in multiple impinging jet arrays. *Journal of Fluid Mechanics*, 546, 255–284. <https://doi.org/10.1017/S002211200500710X>
- Gil, P., & Wilk, J. (2020). Heat transfer coefficients during the impingement cooling with the use of synthetic jet. *International Journal of Thermal Sciences*, 147, 106132. <https://doi.org/10.1016/j.ijthermalsci.2019.106132>
- Hadipour, A., & Rajabi Zargarabadi, M. (2018). Heat transfer and flow characteristics of impinging jet on a concave surface at small nozzle to surface distances. *Applied Thermal Engineering*, 138, 534–541. <https://doi.org/10.1016/j.applthermaleng.2018.04.086>
- Hassan, A. A., & Ismael, M. A. (2023). Fluid-structure interaction of a sweeping impingement jet for cooling hot flat target. *International Journal of Thermal Sciences*, 190, 108323. <https://doi.org/10.1016/j.ijthermalsci.2023.108323>
- He, C. X., & Liu, Y. Z. (2018). A dynamic detached-eddy simulation model for turbulent heat transfer: Impinging jet. *International Journal of Heat and Mass Transfer*, 127, 326–338. <https://doi.org/10.1016/j.ijheatmasstransfer.2018.06.117>
- Huang, H., Sun, T., Zhang, G., Li, D., & Wei, H. (2019). Evaluation of a developed SST $k-\omega$ turbulence model for the prediction of turbulent slot jet impingement heat transfer. *International Journal of Heat and Mass Transfer*, 139, 700–712. <https://doi.org/10.1016/j.ijheatmasstransfer.2019.05.058>
- Hussain, S., Ismael, M. A., & Chamkha, A. J. (2020). Impinging jet into an open trapezoidal cavity partially filled with a porous layer. *International Communications in Heat and Mass Transfer*, 118, 104870. <https://doi.org/10.1016/j.icheatmasstransfer.2020.104870>
- Ismael, M. A., Younes, O., Fteiti, M., Ghalambaz, M., & Homod, R. Z. (2023). Impingement jets on a confined assembly of rotating hot cylinder covered by a surface porous layer. *Applied Thermal Engineering*, 229, 120470. <https://doi.org/10.1016/j.applthermaleng.2023.120470>
- Kalifa, R. B., Habli, S., Saïd, N. M., Bournot, H., & Palec G. L. (2016). Parametric analysis of a round jet impingement on a heated plate. *International Journal of Heat and Fluid Flow*, 57, 11–23. <https://doi.org/10.1016/j.ijheatfluidflow.2015.11.005>
- Kuraan, A. M., Moldovan, S. I., & Choo, K. (2017). Heat transfer and hydrodynamics of free water jet impingement at low nozzle-to-plate spacings. *International Journal of Heat and Mass Transfer*, 108, 2211–2216. <https://doi.org/10.1016/j.ijheatmasstransfer.2017.01.084>
- Lyu, Y. W., Zhang, J. Z., Liu, X. C., & Shan, Y. (2019). Experimental study of single-row chevron-jet impingement heat transfer on concave surfaces with different curvatures. *Chinese Journal of Aeronautics*, 32, 2275–2285. <https://doi.org/10.1016/j.cja.2019.07.002>
- Nagesha, K., Srinivasan, K., & Sundararajan, T. (2019). Enhancement of jet impingement heat transfer using surface roughness elements at different heat inputs. *Experimental Thermal and Fluid Science*, 112, 109995. <https://doi.org/10.1016/j.expthermflusc.2019.109995>
- Pachpute, S., & Premachandran, B. (2018). Effect of the shape of flow confinement on turbulent slot jet impingement cooling of a heated circular cylinder. *International Journal of Thermal Sciences*, 131, 114–131. <https://doi.org/10.1016/j.ijthermalsci.2018.05.026>
- Pachpute, S., & Premachandran, B. (2020). Turbulent multi-jet impingement cooling of a heated circular cylinder. *International Journal of Thermal Sciences*, 148, 106167. <https://doi.org/10.1016/j.ijthermalsci.2019.106167>
- Qiu, T., Song, X., Lei, Y., Dai, H. F., Cao, C. L., Xu, H., & Feng, X. (2016). Effect of backpressure on nozzle inner flow in fuel injector. *Fuel*, 173, 79–89. <https://doi.org/10.1016/j.fuel.2016.01.044>
- Qiu, T., Wang, K. X., Lei, Y., Wu, C. L., Liu, Y. W., Chen, X. Y., & Guo, P. (2018). Investigation on effects of backpressure on submerged jet flow from short cylindrical orifice filled with diesel fuel. *Energy*, 162, 964–976. <https://doi.org/10.1016/j.energy.2018.08.012>
- Sexton, A., Punch, J., Stafford, J., & Jeffers, N. (2018). The thermal and hydrodynamic behaviour of confined, normally impinging laminar slot jets. *International Journal of Heat and Mass Transfer*, 123, 40–53. <https://doi.org/10.1016/j.ijheatmasstransfer.2018.02.083>
- Tang, Z. G., Deng, F., Wang, S. C., & Cheng, J. P. (2021). Numerical simulation of flow and heat transfer characteristics of a liquid jet impinging on a cylindrical cavity heat sink. *Journal of Applied Fluid Mechanics*, 14, 723–732. <https://doi.org/10.47176/jafm.14.03.31945>
- Terzis, A. (2016). On the correspondence between flow structures and convective heat transfer augmentation for multiple jet impingement. *Experiments in Fluids*, 57, 1–14. <https://doi.org/10.1007/s00348-016-2232-7>
- Thani, M. A., & Ismael, M. A. (2022). Numerical study of jet impingement on heated sink covered by a porous layer. *Basrah Journal for Engineering Sciences*, 22, 1–9. <https://doi.org/10.33971/bjes.22.2.1>
- Yeom, T., Huang, L. Z., Zhang, M., Simon, T., & Cui, T. H. (2019). Heat transfer enhancement of air-cooled heat sink channel using a piezoelectric synthetic jet

- array. *International Journal of Heat and Mass Transfer*, *143*, 118484. <https://doi.org/10.1016/j.ijheatmasstransfer.2019.118484>
- Yu, J., Peng, L., Bu, X. Q., Shen, X. B., Lin, G. P., & Bai, L. Z. (2018). Experimental investigation and correlation development of jet impingement heat transfer with two rows of aligned jet holes on an internal surface of a wing leading edge. *Chinese Journal of Aeronautics*, *31*, 1962–1972. <https://doi.org/10.1016/j.cja.2018.07.016>
- Yu, P. P., Zhu, K. Q., Shi, Q., Yuan, N. Y., & Ding, J. N. (2017). Transient heat transfer characteristics of small jet impingement on high-temperature flat plate. *International Journal of Heat and Mass Transfer*, *114*, 981–991. <https://doi.org/10.1016/j.ijheatmasstransfer.2017.06.112>
- Zhang, Y. Y., Li, P., & Xie, Y. H. (2018). Numerical investigation of heat transfer characteristics of impinging synthetic jets with different waveforms. *International Journal of Heat and Mass Transfer*, *125*, 1017–1027. <https://doi.org/10.1016/j.ijheatmasstransfer.2018.04.120>
- Zhao, Y. L., Zhou, Y. Y., & Zhao, Y. X. (2022). Experimental study of the unstart/restart process of a two-dimensional supersonic inlet induced by backpressure. *Journal of Applied Fluid Mechanics*, *15*, 415–426. <https://doi.org/10.47176/jafm.15.02.33220>